Title

Erratum: Subcellular metal imaging identifies dynamic sites of Cu accumulation in Chlamydomonas



Journal

Nature Chemical Biology, 11(3)

ISSN

1552-4450

Authors

Hong-Hermesdorf, Anne
Miethke, Marcus
Gallaher, Sean D
et al.

Publication Date

2015-03-01

DOI

10.1038/nchembio0315-235c

Peer reviewed

ARTICLE
PUBLISHED ONLINE: 26 OCTOBER 2014 | DOI: 10.1038/NCHEMBIO.1662

nature chemical biology

# Subcellular metal imaging identifies dynamic sites of Cu accumulation in *Chlamydomonas*

Anne Hong-Hermesdorf[1,8], Marcus Miethke[1,8], Sean D Gallaher[1], Janette Kropat[1], Sheel C Dodani[2,3], Jefferson Chan[2,3], Dulmini Barupala[4], Dylan W Domaille[2,3], Dyna I Shirasaki[5], Joseph A Loo[1,5,6], Peter K Weber[7], Jennifer Pett-Ridge[7], Timothy L Stemmler[4], Christopher J Chang[2,3] & Sabeeha S Merchant[1,6]*

**We identified a Cu-accumulating structure with a dynamic role in intracellular Cu homeostasis. During Zn limitation, *Chlamydomonas reinhardtii* hyperaccumulates Cu, a process dependent on the nutritional Cu sensor CRR1, but it is functionally Cu deficient. Visualization of intracellular Cu revealed major Cu accumulation sites coincident with electron-dense structures that stained positive for low pH and polyphosphate, suggesting that they are lysosome-related organelles. Nano–secondary ion MS showed colocalization of Ca and Cu, and X-ray absorption spectroscopy was consistent with $Cu^+$ accumulation in an ordered structure. Zn resupply restored Cu homeostasis concomitant with reduced abundance of these structures. Cu isotope labeling demonstrated that sequestered $Cu^+$ became bioavailable for the synthesis of plastocyanin, and transcriptome profiling indicated that mobilized Cu became visible to CRR1. Cu trafficking to intracellular accumulation sites may be a strategy for preventing protein mismetallation during Zn deficiency and enabling efficient cuproprotein metallation or remetallation upon Zn resupply.**



Many proteins in cells are associated with metal ions, which provide structural stability and catalytic functionalities like those of electrophiles, reductants and oxidants that are not readily provided by functional groups of amino acids[1]. Nature has used the unique chemical properties of each metal ion, such as ligand preferences, coordination geometries and redox potential, to generate an amazing repertoire of catalytic abilities, such as the reduction of dinitrogen to ammonium and the oxidation of water, under gentle biological conditions. These catalytic activities are dependent on specific metal cofactors in unique active sites, and life is therefore dependent on the bioavailability of a combination of metal ions. It is critical that the right metal cofactor occupies specifically its dedicated active site. The divalent metal ions of Mn, Fe, Co, Ni, Cu and Zn bind functional groups in proteins according to thermodynamic preferences described by the Irving-Williams series[2], which means that without a mechanism for selectivity *in vivo*, metal binding would be driven by the concentration of the metal ion and the Irving-Williams preferences toward the available binding sites[3,4]. The best-understood mechanisms for ensuring selectivity of metal-protein association include the function of the metallochaperones (prototypes are the Cu chaperones Atx1 and Ccs[5,6]), which effect transfer of the metal to its final target site via specific protein-protein interactions and ligand exchange, and compartmentalized assembly (with MncA as a prototype)[7], in which holoprotein formation is restricted to a compartment with the appropriate high concentration of the desired metal ion and low concentration of an undesired but thermodynamically preferred metal ion[7–9]. Kinetic barriers generally preclude metal exchange or dissociation once the metalloprotein is in its final subcellular location.

As $Cu^{2+}$ is at the top of the Irving-Williams series and $Cu^+$ also has strong preferences for soft ligands such as thiolates, most intracellular compartments maintain very low concentrations of 'free' Cu ions[10]. For instance, *C. reinhardtii*, a eukaryotic reference organism for studying metal homeostasis in the context of chloroplast biology, maintains a Cu quota that is determined strictly by the abundance of various cuproproteins required for its metabolism, especially plastocyanin for photosynthesis, cytochrome (Cyt) oxidase for respiration and a ferroxidase for iron assimilation, even when presented with 100-fold excess Cu in the growth milieu[11,12]. This quota is achieved by restricted Cu uptake. In Cu-deficient conditions, *C. reinhardtii*, like other algae and many cyanobacteria, can reduce the Cu quota substantially by substituting a heme protein, Cyt $c_6$, for plastocyanin[13,14]. The reciprocal accumulation of Cyt $c_6$ versus plastocyanin as a function of medium Cu content serves as a readout of the Cu nutritional state and is effected by a transcriptional program dependent on a Cu-sensing SBP-domain transcription factor called CRR1 (refs. 15,16).

Cu homeostasis in *C. reinhardtii* is disrupted by nutritional Zn deficiency, which results in unprecedented Cu accumulation of up to 20 times the typical quota[17]. In this work, we used high-resolution secondary ion MS (SIMS) with a NanoSIMS 50 to localize Cu in intracellular compartments[18,19] reminiscent of the acidocalcisome and the previously described zincosomes[20–22]. The accumulated $Cu^+$ was in a reproducibly organized chemical environment consisting of N, S and O ligands, but it became bioavailable with priority over extracellular Cu for deactivating CRR1 and metallating apoplastocyanin. We hypothesize that compartmentalization would prevent mismetallation of Zn enzymes, but this would result in intracellular Cu deficiency, which would activate CRR1, resulting in feed-forward

[1]Department of Chemistry and Biochemistry, University of California–Los Angeles, Los Angeles, California, USA. [2]Department of Chemistry, University of California–Berkeley, Berkeley, California, USA. [3]Howard Hughes Medical Institute, University of California–Berkeley, Berkeley, California, USA. [4]Department of Pharmaceutical Sciences, Wayne State University, Detroit, Michigan, USA. [5]Department of Biological Chemistry, University of California–Los Angeles, Los Angeles, California, USA. [6]Institute for Genomics and Proteomics, University of California–Los Angeles, Los Angeles, USA. [7]Chemical Sciences Division, Lawrence Livermore National Laboratory, Livermore, USA. [8]These authors contributed equally to this work. *e-mail: merchant@chem.ucla.edu

overaccumulation. Compartmentalized sequestration of accumulated $Cu^+$ instead of cellular efflux, which dominates in bacterial systems as a means of detoxification[23–25], allowed the storage of this metal ion for future use in a situation of challenging micronutrient availability.

## RESULTS

### Zn deficiency disrupts Cu homeostasis

*C. reinhardtii* keeps intracellular Cu content relatively constant between ~1 × $10^7$ and 2.5 × $10^7$ atoms per cell when the external milieu contains chelated Cu ranging from 1 µM to 80 µM (ref. 12), but this fine-tuned homeostatic mechanism is disrupted in Zn-limited cells[17]. Zn-limited cells showed a growth phenotype, especially in the second round of cultivation in limited medium (**Supplementary Results**, **Supplementary Fig. 1**). Inductively coupled plasma (ICP)-MS analysis (**Fig. 1**) of these cells showed marked accumulation of Cu to up to ~30 × $10^7$ atoms per cell in standard growth medium containing 2 µM $Cu^{2+}$-EDTA (**Fig. 1a**). If the external supply was increased from 2 µM to 50 µM, intracellular Cu content was further enhanced to ~40 × $10^7$ atoms per cell (**Fig. 1b**). Hyperaccumulation occurred only in *CRR1* but not *crr1* cells, indicating that the pathway is dependent on the nutritional Cu regulon (**Fig. 1c**). Indeed, the CTR transporters, which provide the route for $Cu^+$ assimilation, were upregulated in Zn-limited cells despite adequate extracellular $Cu^{2+}$ and excessive intracellular $Cu^+$ (see below).

### Biological but not chemical Cu deficiency

To distinguish the underlying mechanism, we monitored the expression of sentinel genes of the Cu regulon by quantitative PCR with reverse transcription (qRT-PCR). Expression of *CYC6* (encoding Cyt $c_6$), whose transcripts are completely absent in Cu- and Zn-replete cells, was markedly increased in Zn-limited cells (**Fig. 2a**), as was the corresponding protein (**Fig. 2b**). In contrast, the abundance of plastocyanin was substantially reduced in Zn-limited cells, just as it was in Cu-deficient ones (**Fig. 2b**), indicating functional Cu deficiency. This situation would activate the expression of the assimilatory CTR-family $Cu^+$ transporters via CRR1 and in so doing would account for the concentration-dependent hyperaccumulation of Cu. We conclude that Zn-limited cells experience biological but not chemical Cu deficiency.

We observed that the Zn content was only slightly increased (about 2.5-fold) in Cu-depleted versus Cu-replete cells (**Fig. 1d**), possibly because of increased expression of *IRT2* (encoding iron responsive transporter 2 of the ZIP family[26]). This finding is consistent with the expression of sentinel genes of the Zn regulon, *ZRT3* and *ZRT5* (ref. 17) (encoding Zn-responsive transporters of the ZIP family) only in Zn-limited but not Cu-deficient cells (**Fig. 2a**).

### Cu accumulates in foci and colocalizes with Ca

In pilot survey experiments to screen whether Cu might be sequestered (i.e., be biologically inaccessible) in Zn-deficient *C. reinhardtii* cells, we used fluorescence imaging with a pair of structurally and functionally matched fluorophores (**Fig. 3a**), where one has the capability to respond to Cu and the other does not (**Supplementary Fig. 2a–c**). Cu sensor-3 (CS3)[27], the Cu-responsive dye, showed a selective and high turn-on response to Cu (75-fold) and a tighter $K_d$ for $Cu^+$ ($K_d = 9 \times 10^{-14}$) relative to glutathione (GSH), an abundant competing cellular ligand (apparent $K_d = 9 \times 10^{-12}$ (ref. 28), assuming the major species is a 1:1 Cu–GSH complex)[29]. CS3 did not respond to pH alone and retained the ability to respond to Cu in the pH range of 4 to 7.5 (**Supplementary Fig. 2b**), which makes it suitable for staining intracellular compartments. Ctrl-CS3 (**1**) used an identical BODIPY fluorophore to that of CS3 and has the exact same number of receptor atoms (**Supplementary Fig. 2a**), except that the four sulfur atoms that are essential for metal interaction in CS3

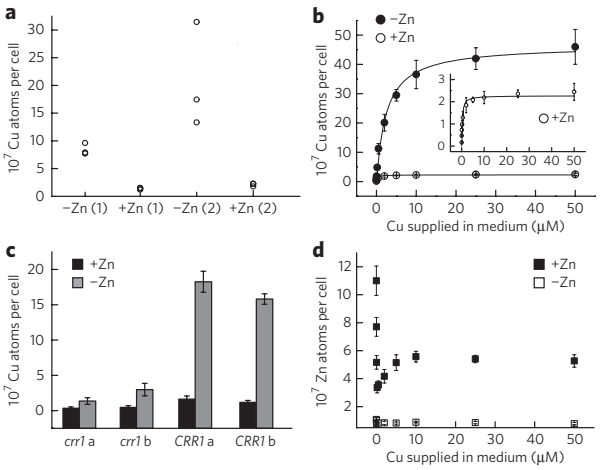


**Figure 1 | Zn deficiency induces CRR1-dependent Cu hyperaccumulation.** ICP-MS analysis of Cu and Zn contents in cells grown under Zn-limited (−Zn) or Zn-replete (+Zn) conditions. (**a**) Cellular Cu contents in cells from three independent *C. reinhardtii* cultures (strain CC-4532) that were grown to mid-logarithmic phase in either −Zn or +Zn (containing 2.5 µM $ZnCl_2$) TAP medium (in the first (1) and second (2) round of transfer to indicated medium). (**b**,**d**) Quantification of Cu (**b**) and Zn (**d**) contents in cells grown under a concentration range of supplemented Cu (0 µM, 0.02 µM, 0.05 µM, 0.2 µM, 0.5 µM, 2 µM, 5 µM, 10 µM, 25 µM and 50 µM) in −Zn or +Zn TAP medium. The inset in **b** is the rescaled representation of Cu contents in the Zn-replete cells. The difference in total Cu content between −Zn and +Zn cells is about 20-fold. (**c**) Cu contents in *crr1-2* frameshift mutants[16] (CC-3960) and *CRR1* complemented strains (a and b represent two independent isolates). Quantification results are from three different experiments per strain, and conditions are shown as separate data points (**a**) or as averages with corresponding s.d. (**b**–**d**).

are replaced by isosteric carbons that lack affinity for Cu binding (**Fig. 3a**). Indeed, Ctrl-CS3 did not respond to Cu or pH changes, as demonstrated by Cu and pH titration assays (**Supplementary Fig. 2c**) and thus could be used in conjunction with CS3 to distinguish between Cu-dependent versus any potential dye backbone–dependent responses.

Confocal fluorescence microscopy with CS3 but not with its Ctrl-CS3 counterpart, which does not respond to Cu, showed the presence of fluorescent foci that correlated with the Zn deficiency status of the cells (**Fig. 3b**); the foci were not as frequently observed in Zn-replete cells (**Fig. 3b**). More notably, fluorescent foci were seen only in situations where ICP-MS methods indicated high intracellular Cu content. Specifically, the fluorescent foci were not observed in cells of the *crr1* mutant, which cannot hyperaccumulate Cu, but were readily visualized in Zn-limited cells of the complemented strain (**Supplementary Fig. 3a**). The CS3 signal was markedly reduced when cells were treated with a cell-permeant Cu chelator, GSH monoethyl ester, before staining with CS3 (**Supplementary Fig. 3b**). Multiple control experiments were performed to ensure the specificity of CS3 for $Cu^+$ in this model system (**Supplementary Note** and **Supplementary Fig. 20**).

Because CS3 is based on a lipophilic BODIPY platform[27], there was concern that the probe might be staining lipid bodies, which accumulate in Zn-deficient cells[30], and so we performed multiple lines of control experiments to address this potential issue. First, the Ctrl-CS3 dye, which lacks the Cu-binding atoms but retains the same lipophilic dye platform, did not stain the putative Cu puncta or any other body in Zn-deficient cells (**Fig. 3b**). We also tested whether CS3 would visualize lipid bodies in N-deficient *C. reinhardtii* cells,

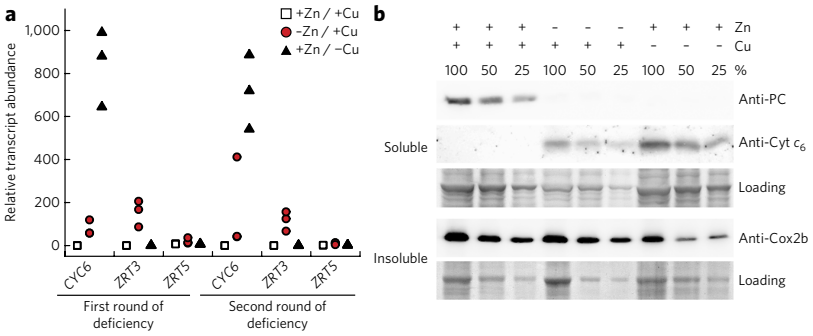


**Figure 2 | Zn-limited cells also express Cu deficiency markers.** (**a**) qRT-PCR was used to test for the expression of genes that react to altered Zn and Cu availability, respectively. The tested genes were *CYC6*, which encodes Cyt $c_6$ as a marker for the Cu-deficiency regulon, and *ZRT3* and *ZRT5*, which encode ZIP transporters as markers of the Zn-deficiency regulon. The relative transcript abundance is calculated with the LinRegPCR program and is plotted as separate data points for triplicate cultures grown either under replete conditions (+Zn +Cu), Zn deficiency (−Zn +Cu) or under Cu deficiency (+Zn −Cu) in the first and second round of limitation, respectively. (**b**) Immunoblot analyses showed that Cyt $c_6$ and plastocyanin (PC) were adjusted in Zn-deficient cells to levels expected from Cu-deficient cells. Shown are immunoblots with dilution series (100%, 50% and 25%) of soluble and insoluble protein extracts that were incubated with anti-PC, anti-Cyt $c_6$, and an antibody against a Cu-binding subunit of Cyt oxidase (anti-Cox2b), respectively. This experiment was carried out three times, and a representative set of those is shown. Full Coomassie blue-stained gels of loading controls are shown in **Supplementary Figure 18**.

which hyperaccumulate lipids but do not hyperaccumulate Cu. We found that lipid bodies in N-deficient cells, which do stain well with Nile Red, did not stain with CS3 in parallel experiments with the same settings (**Supplementary Fig. 4**).

With these pilot data suggesting further investigation, we sought to use an unequivocal physical technique to identify the intracellular Cu foci. Direct metal detection techniques such as X-ray fluorescence microscopy have been valuable to support indirect metal imaging obtained using synthetic fluorophores[27]. In the present study, electron-dense structures were revealed in microtomed thin sections of fixed cells by TEM, and these were candidate sites for Cu accumulation. Indeed, the abundance and size of the electron-dense structures correlated with Zn nutrition (**Fig. 4a**). Kruskal-Wallis one-way analysis of variance on ranks of the electron-dense areas in the electron micrographs in relation to total cell areas found a significant difference between the Zn-limited and Zn-replete sections ($P < 0.001$; **Fig. 4a**). NanoSIMS imaging, which allows simultaneous spatial detection of elements based on their mass, indicated that regions containing Ca and Cu correlated with electron-dense structures at the periphery of the cells visible in scanning electron microscopy (STEM) images of the same sections (**Fig. 4b**). Colocalization of Ca and Cu in Zn-limited cells was confirmed independently by confocal microscopy and dual staining of cells with CS3 and Fluo-4 AM, a $Ca^{2+}$-specific fluorescent dye (**Supplementary Fig. 5**).

To test the relationship between sites of Cu concentration and Zn deficiency, we resupplied $Zn^{2+}$ to cultures of Zn-limited cells and sampled over a 24-h time course for NanoSIMS analysis of thin sections. We noted a decrease in Cu abundance over time at the foci of Cu concentration as well as over the total cell area (**Fig. 4c–e**), agreeing with the ICP-MS measurements showing Cu accumulation only under strict Zn limitation. This observation suggests further that Cu can be mobilized from the sites of concentration (see below).

## Compartmentalized $Cu^+$ is stabilized by O and/or N and S ligands

We recorded Cu K-edge X-ray absorption near edge structure (XANES) spectra, which provide information about the average electronic state and ligand symmetry of the metal, on Zn-limited *C. reinhardtii* cells (**Fig. 4f**). The spectra showed a highly reproducible pre-edge feature centered at 8,984 eV, which is typically attributed to $1s \rightarrow 4p$ electronic transitions in centrosymmetric $Cu^+$ environments; the intensity of this feature also provides insight into the cuprous coordination geometry, which was indicative of 2 or 3 coordinate $Cu^+$. The absence of any appreciable feature at 8,980 eV in the Cu pre-edge XANES, a feature attributed to the $1s \rightarrow 3d$ transition in $Cu^{2+}$, suggests that $Cu^{2+}$ in these samples was limited (**Fig. 4g**). On the basis of the model pre-edge XANES analysis, we expected that $Cu^{2+}$ contamination in the samples would have been noticeable had it been present at ≥15% proportion. We therefore estimate that these structures are at least 85% $Cu^+$ (ref. 31).

Extended X-ray absorption fine structure (EXAFS) simulations on the same sample allowed us to determine the average metrical parameters for the ligand environment of the cuprous metal. EXAFS simulations showed that Cu is coordinated in its nearest neighboring

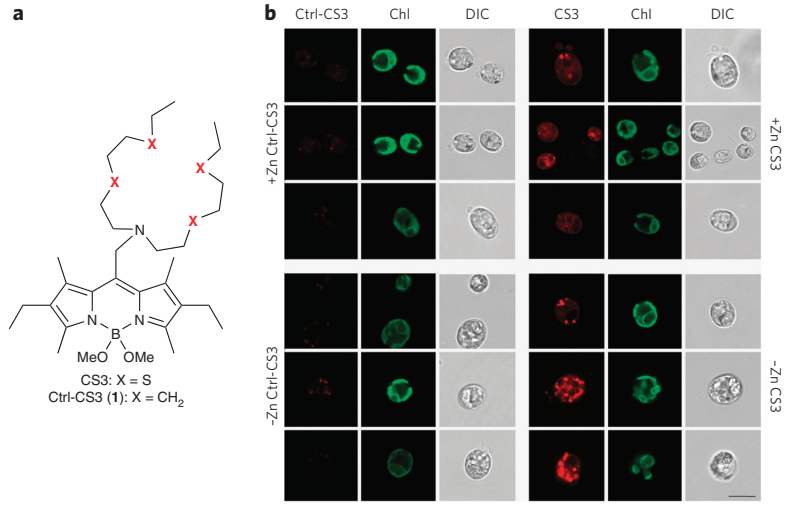


**Figure 3 | $Cu^+$-sensitive CS3 staining suggests Cu accumulation in intracellular compartments.** (**a**) Chemical structure of the $Cu^+$-binding fluorescent dye CS3 and the non-copper-binding analog Ctrl-CS3, in which the four metal-binding S atoms are replaced by isosteric carbons. Detailed synthesis is described in **Supplementary Note** and **Supplementary Figure 2a**. (**b**) Zn-limited and Zn-replete wild-type *C. reinhardtii* (CC-4532) cells were stained with the cuprous dye CS3 (ref. 25) to observe intracellular Cu distribution by confocal microscopy. As a control, we stained cells from the same cultures with the control dye Ctrl-CS3. DIC, differential interference contrast; Chl, chlorophyll autofluorescence. Scale bar, 10 µm. In total, we analyzed 55 Zn-deficient cells stained with CS3, 30 Zn-deficient cells treated with Ctrl-CS3, 54 Zn-replete cells stained with CS3 and 64 Zn-replete cells treated with Ctrl-CS3.

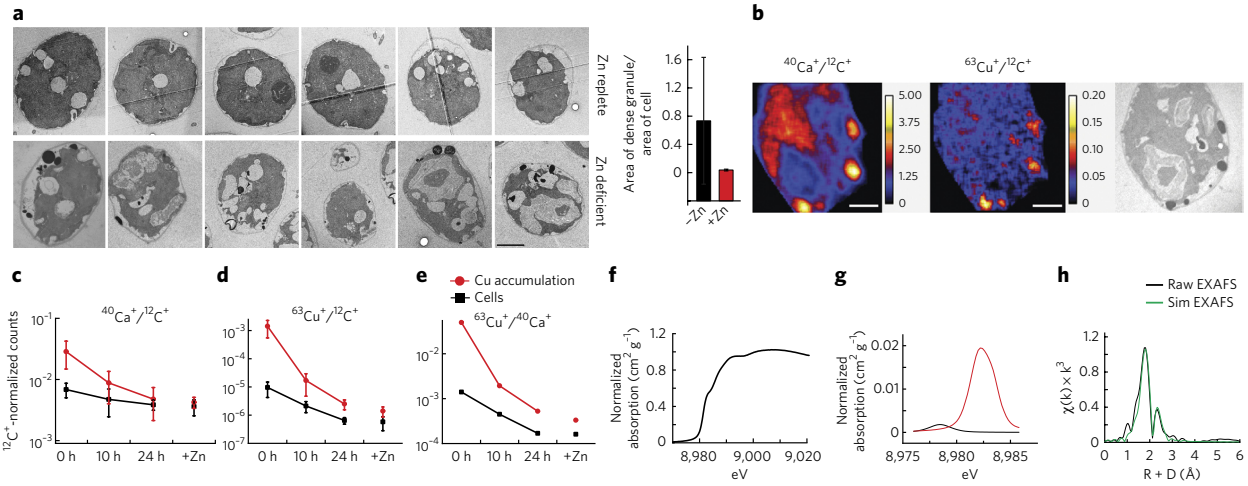


**Figure 4 | Intracellular Cu is traceable to Cu-accumulating compartments.** (**a**) TEM revealed electron-dense structures in Zn-limited cells. Manually defined areas of cells and the contained electron-dense structures were measured with ImageJ. We analyzed the statistical significance of Zn-limited versus Zn-replete cells by Kruskal-Wallis one-way analysis of variance on ranks ($P < 0.001$). Error bars show ± s.d. from three independent experiments. Scale bar, 2 µm. (**b**) NanoSIMS shows that $^{40}Ca^+$ and $^{63}Cu^+$ colocalize in Zn-limited cells, coinciding with electron-dense structures in STEM. Scale bars, 1 µm. (**c**,**d**) Relative intracellular Ca (**c**) and Cu (**d**) measured during Zn resupply (to −Zn compared to +Zn). Samples from three independent cultures were collected 0 h, 10 h and 24 h after Zn addition (denoted as +Zn), and ten cells per time point were examined by NanoSIMS. Average ion ratios were plotted on the basis of whole cell area ('cell') and intracellular area of Ca and Cu accumulation, with their corresponding s.d. (**e**) Ratio of $^{40}Ca^+$ over $^{63}Cu^+$ at different time points. All NanoSIMS counts were normalized to $^{12}C^+$. (**f**–**h**) XAS spectra for Cu in a representative Zn-limited *C. reinhardtii* sample. (**f**) Cu XANES spectrum with a predominant spectral feature at 8,984 eV, which corresponds to the 1s→4*p* electronic transition typically seen in centrosymmetric $Cu^+$ samples. (**g**) Expansion of the Cu pre-edge spectral features (red) offset and compared to the $CuSO_4$ (black) model representing $Cu^{2+}$. (**h**) Fourier transforms of the raw Cu EXAFS (black) with best-fit simulation (green).

environment by a mixture of O and N as well as S ligands, with long-range scattering attributed to C only. Parameters from the best-fit simulation of the Cu EXAFS (**Supplementary Fig. 6**) indicate that the average metal-ligand coordination environment is constructed by ~2 O and/or N ligands with an average bond length of 2.11 Å and a single resolvable S ligand at 2.3 Å (**Supplementary Table 1**). Long-range scattering ($R > 3$ Å) could be best fit with carbon scattering at 2.75 Å. Attempts to include Cu-Cu scattering were unsupported in these data. These simulation parameters closely match the projected ligand environments observed in the Fourier transform of the sample Cu EXAFS (**Fig. 4h**) and the coordination geometry was similar to that seen in the M site in peptidylglycine monooxygenase at low pH[32].

## Enrichment of the Cu-containing compartment

To determine whether $Cu^+$ is concentrated in a compartment, we used biochemical fractionation methods to enrich cell fractions based on Cu and Ca content. Zn-replete and Zn-limited cells were disrupted by grinding in the presence of silicon carbide particles, followed by density gradient centrifugation. The Cu- and Ca-containing fractions contained small 'bodies' with an average diameter of 0.2 µm after they were dispersed in detergent-containing buffered solutions. Without detergent, the bodies, which were much more abundant in extracts of Zn-limited cells, had a tendency to form large aggregates, even upon vigorous vortexing. Elemental analysis of EDTA-washed bodies indicated that they also contained P, independent of cellular Zn content, and were indeed enriched in Cu and Ca when isolated from Zn-limited cells (**Supplementary Fig. 7**). Staining with CS3 also indicated that the bodies isolated from Zn-limited cells were highly enriched in $Cu^+$ compared to Zn-replete cells (**Supplementary Fig. 8**).

Staining with 4′,6-diamidino-2-phenylindole (DAPI) and monitoring polyphosphate-specific fluorescence emission between 500 nm and 550 nm (ref. 33) suggested the presence of this polymer in the isolated fraction (**Supplementary Fig. 9**), which may represent the electron-dense material visible by TEM. Fixed cells from Zn-limited cultures showed bright and larger areas of DAPI staining in the polyphosphate-specific emission range, whereas smaller foci were present at lower abundance in Zn-replete cells (**Supplementary Fig. 9a**). Hence, size and abundance of intracellular polyphosphate-containing bodies, which were purified on the basis of Cu and Ca content, correlated with the electron-dense TEM structures observed in *C. reinhardtii* cells (**Fig. 4a**).

When we stained the fraction enriched for the Cu- and Ca-containing bodies with LysoSensor Green DND-189 ($pK_a$ ~5.2), which has increased fluorescence intensity at low pH, we noted staining in the isolated bodies, with higher intensity in Cu-containing compartments isolated from Zn-limited cells, suggestive of lower pH in the bodies during low Zn growth (**Supplementary Fig. 8**). Indeed, the specific activity of a characteristic marker of the acidocalcisomes, $H^+$-PPase[20,34], was slightly higher in the fraction from Zn-limited cells (**Supplementary Fig. 10a**) and had a dose-dependent response to specific inhibitors[34,35] (**Supplementary Fig. 10b**). Further, staining of whole cells with CS3 together with the membrane-permeable pH sensor ageladine A[36] confirmed a general colocalization of $Cu^+$ accumulation and acidic intracellular compartments, which were more abundant in Zn-limited cells (**Supplementary Fig. 9b**). Taken together, we conclude that the Cu-containing compartment is analogous to the previously described acidocalcisome, which is a lysosome-related organelle[20,37]. The metal content of this compartment was dynamic, as evidenced by increased Mg and Zn in the fraction purified from Zn-replete cultures relative to the Zn-limited culture (**Supplementary Fig. 7c**).

## Accumulated Cu is bioavailable

To test whether Cu in the compartment could be released, we resupplied Zn-limited cells with $ZnCl_2$ and used CS3 in a pilot

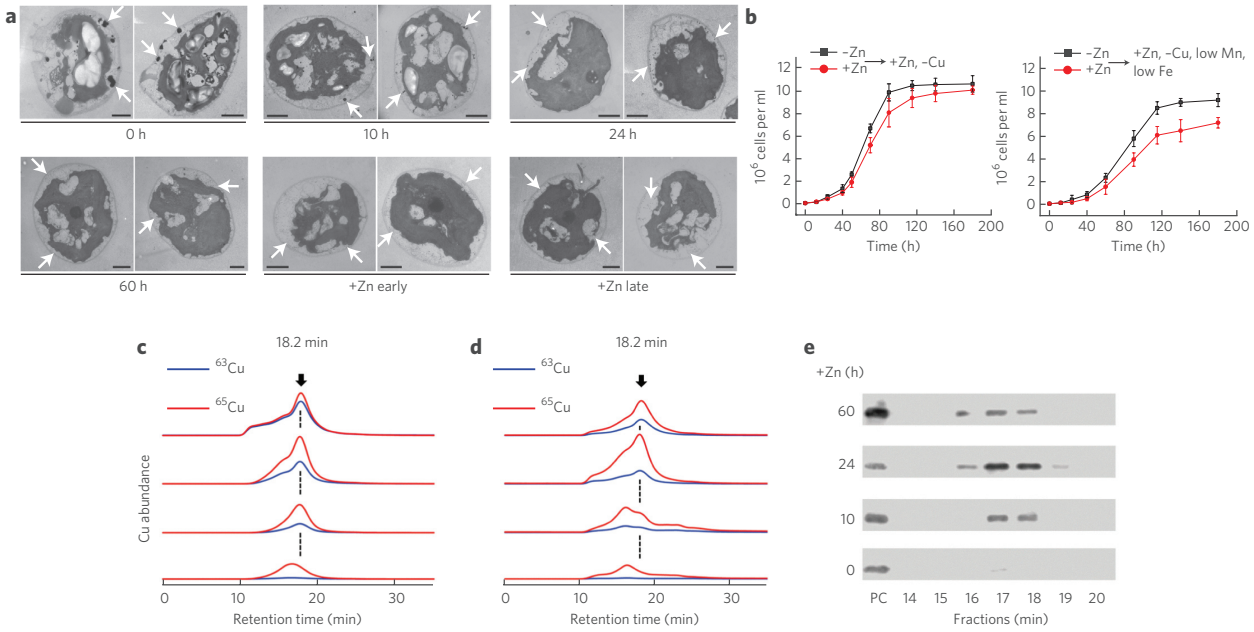


**Figure 5 | Changes in abundance of electron-dense bodies and Cu redistribution upon Zn resupply.** (**a**) Electron microscopy of Zn-limited cells during Zn resupply (0 h, 10 h, 24 h and 60 h after addition of $ZnCl_2$, denoted as '+Zn') and Zn-replete cells in early and late logarithmic growth phases (+Zn early and +Zn late). Two representative specimens from three independent cultures are shown for each condition. Arrows point to electron-dense bodies, mainly in the periphery of the cells. Scale bars, 2 μm. (**b**) Growth curves of Zn-limited or replete cells, which were inoculated into fresh TAP medium containing $ZnCl_2$ but no Cu (left) or no Cu and 0.1 μM Mn and 0.5 μM Fe (right). Mean values of three independent experiments with corresponding s.d. are shown. (**c**–**e**) $^{65}$Cu-labeled cells grown under Zn limitation were supplied with $^{63}$Cu (10 μM $^{63}CuCl_2$) either together with Zn resupply (**c**) or 5 h after Zn resupply (**d**). Soluble proteins were extracted anaerobically at 0 h, 10 h, 24 h and 60 h after Zn addition and analyzed by LC-ICP-MS to monitor the Cu isotope content of the protein species. This experiment was performed twice using $^{65}$Cu as the label and chasing with $^{63}$Cu and twice using $^{63}$Cu as the label and chasing with $^{65}$Cu. Shown are the ion chromatograms for Cu isotopes $^{63}$Cu and $^{65}$Cu. The emerging Cu isotope peak at 18.2 min corresponds to plastocyanin (PC)-associated Cu. The corresponding LC fractions were analyzed by immunoblotting for their plastocyanin contents. (**e**) Immunoblot analysis of respective fractions with purified plastocyanin from *C. reinhardtii* as standard.



experiment to monitor intracellular Cu-containing compartments. Fluorescent foci decreased starting at ~3–4.5 h after $Zn^{2+}$ resupply, and fluorescence became more homogenously distributed throughout the cell by about 24 h (**Supplementary Fig. 11**). This correlated with a decrease in the abundance and size characteristic of electron-dense structures in Zn-limited cells (**Fig. 5a**), consistent with these structures being related to sites of Cu accumulation. To test whether the released $Cu^+$ was bioavailable, we moved Zn-limited ($Cu^+$-accumulating) cells to Zn-replete but Cu-deficient growth medium and found that these cells had higher growth rates compared to cells shifted from Zn-replete (not $Cu^+$-accumulating) to Cu-deficient conditions, presumably because the former had access to an internal $Cu^+$ reservoir (**Fig. 5b**). This effect was even more notable when the new medium was depleted also for Mn and Fe, which also accumulated slightly (two- to threefold) in Zn-limited cells (**Fig. 5b** and **Supplementary Fig. 12**).

To document the use of accumulated $Cu^+$ for *de novo* synthesis of a cuproprotein, we labeled Zn-limited cells with isotopically enriched Cu ($^{63}$Cu or $^{65}$Cu), and then we added a fivefold excess of the other Cu isotope, either simultaneously with Zn resupply (**Fig. 5c**) or 5 h after Zn resupply (**Fig. 5d**). We separated plastocyanin and monitored polypeptide abundance by immunoblotting (**Fig. 5e**) and measured the Cu isotope abundances by ICP-MS. The difference between the peak of eluted plastocyanin, which had a retention time of 16.6 min (17-min fraction), and the plastocyanin-associated peak, which had a retention time of 18.2 min, was due to the time lag between protein detection by the LC multiwavelength detector and Cu detection by the ICP-MS mass analyzer (**Supplementary Fig. 13**). Mass spectrometry enhanced ($MS^E$)-based quantifications of plastocyanin (PC) and Cyt $c_6$ abundances in LC fractions obtained from reciprocal Cu isotope labeling experiments are shown in **Supplementary Figure 14**. Newly synthesized proteins potentially have access to two different pools of Cu: one derived from intracellular Cu-accumulating sites and the other from the growth medium. Resupply of Zn resulted in strong stimulation of growth (**Supplementary Fig. 15a**) and a 200-fold increase in plastocyanin accumulation (**Supplementary Fig. 14**). The Cu associated with newly synthesized plastocyanin showed a 2:1 preference for the isotope species from the intracellular store (**Fig. 5c** and **Supplementary Fig. 15b**). However, 24 h after Zn resupply, the Cu content of the cell included both the intracellular prior accumulation and extracellular oversupplied species in about equal proportion (**Supplementary Fig. 16**). At 60 h after Zn resupply, the extracellularly oversupplied species represented about two-thirds of the intracellular Cu pool, but plastocyanin remained relatively enriched (50/50 mix of both isotopes) for Cu from the intracellular accumulation site (**Fig. 5c** and **Supplementary Figs. 15b** and **16**). We conclude that upon restoration of Cu homeostasis, $Cu^+$ from the internal Cu-accumulating compartment is more readily accessible for metallation of cuproproteins synthesized *de novo*.

When we supplied the other Cu isotope to cells 5 h after Zn resupply rather than simultaneously, we found that the Cu isotope in plastocyanin is enriched 2:1 for the prior compartment-accumulated form even 60 h later (**Fig. 5d** and **Supplementary Fig. 15c**). We attribute this result to the reduced expression of CTR transporters (see below) upon restoration of Cu homeostasis, which results from Cu visibility to CRR1, and hence reduced uptake of externally supplied Cu.

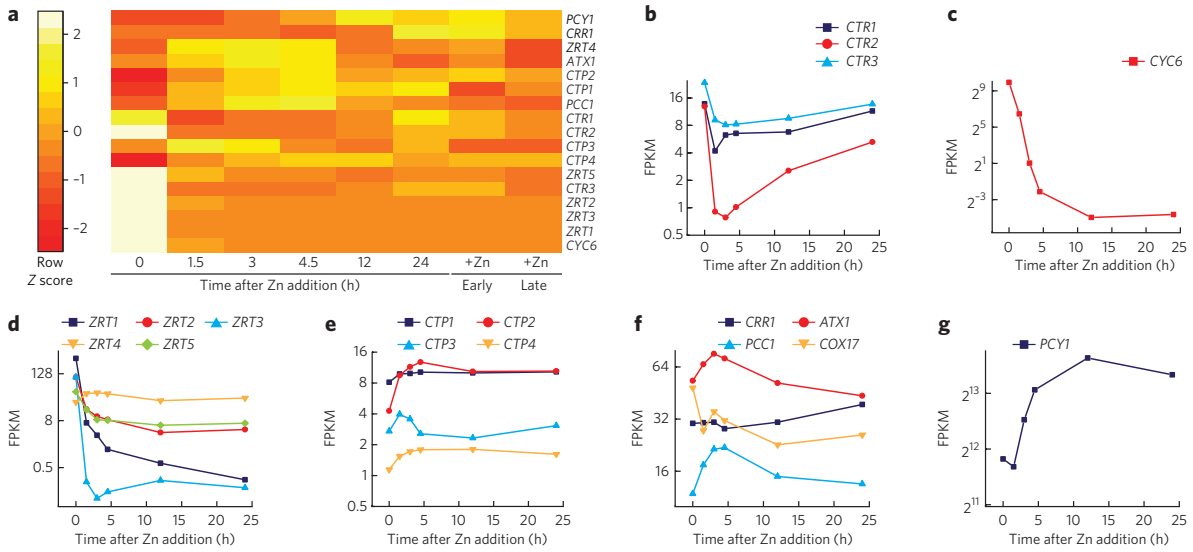


**Figure 6 | Transcriptome response to Zn resupply monitored by RNA-seq analysis.** (**a**) Heat map showing *Z* scores (interpreted as a measure of s.d. away from the mean) for the changes of FPKM of selected genes, indicated on the right. The time points 0–24 h after Zn addition indicate the sampling during Zn resupply to a Zn-limited culture. '+Zn early' and '+Zn late' columns indicate samples from Zn-replete cultures taken in the stages of the early logarithmic and beginning stationary growth phase, respectively. (**b–g**) The mRNA abundance (in FPKM) is given for members of the *CTR* family (**b**); *CYC6* (**c**); genes encoding members of the *ZIP* family (**d**); genes encoding members of the $P_{1B}$-type ATPase family (**e**); CRR1 and Cu chaperones *ATX1*, *PCC1* and *COX17* (**f**); and *PCY1* (plastocyanin) (**g**). The *y* axes of the diagrams are $\log_2$ scaled.



To assess the operation of CRR1, we monitored the transcriptome as a function of Zn resupply (between 0 h and 24 h) by RNA-Seq. A heat map showing individual changes in transcript abundance for 17 genes involved in Cu and Zn homeostasis is presented (**Fig. 6a** and with absolute scaling in **Supplementary Fig. 17a**). The *P* values indicate the significance of changes in fragments per kb of exon per million (FPKM) between time points (**Supplementary Table 2**). *CTR* transcripts were abundant in Zn-limited cells, supporting the contention that $Cu^+$ hyperaccumulation was driven by high CTR expression (**Fig. 6b**). Transcript abundance for all three *CTR* genes decreased rapidly (comparable to the behavior of *CYC6*, a sentinel gene of nutritional Cu signaling) during the first 3–5 h, which is consistent with $Cu^+$ mobilization from the internal compartment (**Supplementary Fig. 11**) and hence deactivation of CRR1 (ref. 16) (**Fig. 6c**). Notably, as intracellular Cu was depleted for synthesis of cuproproteins during growth and division, CRR1 and hence expression of its target genes were reactivated. RNAs encoding the candidate $Zn^{2+}$ transporters, members of the ZIP family, were also rapidly reduced upon $Zn^{2+}$ addition, and those genes remained repressed throughout the time course (**Fig. 6d**).

## Cu homeostasis

The time course experiment also revealed a previously unappreciated effect on the expression of genes for intracellular Cu movement. Transcripts encoding the intracellular 'distributive' CTP transporters, which use ATP hydrolysis to transport copper ions against a concentration gradient, as well as those encoding $Cu^+$ chaperones *ATX1* and *PCC1* (ref. 38), increased in abundance soon after Zn resupply (**Fig. 6e**,**f**), presumably to facilitate Cu distribution to the chloroplast for plastocyanin biosynthesis and to the secretory pathway for biosynthesis of a ferroxidase-ferric transporter complex required for iron uptake[39,40] (**Supplementary Fig. 17b**). We note that transcripts of *PCY1*, *FOX1* and *FTR1*, encoding plastocyanin and proteins involved in the iron uptake pathway, also increased in parallel with increased $Cu^+$ bioavailability (**Figs. 5c** and **6g** and **Supplementary Fig. 17b**). In contrast, the abundance of *COX17* transcripts encoding functions required for Cyt oxidase assembly[41,42] decreased, which is consistent with the lack of change in *COX2A* and *COX3* transcript abundance upon Zn resupply (**Supplementary Fig. 17b**) and the relative stability of Cyt oxidase even in a $Cu^+$-challenged growth condition (**Fig. 2b**).

## DISCUSSION

Typically, the Cu quota of a cell is tightly regulated and determined by the abundance of various cuproproteins, but poor nutrition or genetic mutation can result in misregulation and hence overload of metals. Here, we took advantage of Cu misregulation in Zn-limited cells to analyze sites of Cu sequestration in *C. reinhardtii*. Pilot survey experiments with a pair of matched fluorescent dyes that can (CS3) or cannot (Ctrl-CS3) respond to $Cu^+$ in live-cell imaging experiments led to direct detection of sites of Cu accumulation by imaging MS of fixed, sectioned cells, which localized bound Cu only[44]. In this context, we note that fluorescent probes are a developing technology that should be used with caution and appropriate controls, both genetic and chemical. These reagents are designed and physically characterized by chemists in tightly controlled *in vitro* environments, but biologists may use them in vastly divergent cells and organisms where solubility, intracellular distribution and reactivities can vary. To help address some of these potential issues, we designed an isostructural control compound that can be used to distinguish between dye-dependent and receptor-dependent fluorescence responses in an intracellular environment. Replacement of metal-interacting sulfurs in CS3 with isosteric carbons yields a matched Ctrl-CS3 dye that lacks responsiveness to Cu and pH and represents a new chemical approach for the use of small-molecule sensors *in vivo*. Yet, the presence of more reactive functionalities in CS3 versus Ctrl-CS3 may create unanticipated chemical reactions *in vivo*. The use of appropriate controls cannot be overemphasized. For instance, although CS3 does not stain lipid bodies in *C. reinhardtii* by itself, CS3 (but not Ctrl-CS3) will fluoresce in costaining experiments with some dyes (for example, diphenylhexatriene), possibly because of an interaction between the two dyes dependent on the four S atoms. The precise mechanism by which CS3 responds in *C. reinhardtii* compartments is insufficiently understood, whether

by direct binding or by an unknown $Cu^+$-mediated process, and the fluorescence output is not quantitative. Nevertheless, the dependence of the signal on intracellular Cu content, as directly measured by ICP-MS and Nano-SIMS, and on a functional *CRR1* locus, along with the fact that the isosteric Ctrl-CS3 does not respond to changes in intracellular Cu in these same strains, strengthens the interpretation of the CS3 signal in the models used in this study (**Fig. 3b**). The use of fluorescent probes as a tool for pilot screening in live samples is potentially useful in downstream high-throughput genetic screens now that their validity has been established in this organism with more resource-intensive physical techniques. We note that *in vitro* experiments with small-molecule sensors (**Supplementary Note**) clearly do not faithfully mimic all aspects of their chemistry in a biological setting. Therefore, each probe must be tested in each experimental model accompanied by other chemical and/or genetic controls in that model.

Imaging MS has the caveat that it requires chemical fixation and sectioning of cells and is therefore restricted to analysis of bound elements in that section. We cannot rule out the possibility that there is another pool of $Cu^+$ that neither technique reached. Taken together, both methods support the conclusion that *C. reinhardtii* sequestered Cu under Zn limitation, causing Cu to be unavailable for cuproprotein biosynthesis, and hence *C. reinhardtii* plastocyanin levels (a biomarker for intracellular Cu) were low (**Fig. 2b**). Sequestered $Cu^+$ was also invisible to a Cu-sensing transcription factor, CRR1, which is responsible for maintaining cellular Cu quota[16]. Accordingly, *C. reinhardtii* expressed the nutritional Cu regulon, including the *CTR* genes encoding plasma membrane–localized $Cu^+$ assimilation components[12]. The transporters drew more $Cu^+$ into the cell, and hence $Cu^+$ hyperaccumulated dependently on the external supply and CRR1 (**Fig. 1b**,**c**).

We probed the identity of the Cu accumulation sites on the basis of prior descriptions of acidocalcisomes[20,34]. The acidocalcisome is a low-pH, lysosome-related organelle that contains polyphosphate and metal ions, especially Ca and Fe[37]. Its Cu content had not previously been described, potentially because of the common use of Cu grids for microscopic techniques for metal visualization[34]. Staining of intact cells or enriched compartments with fluorescent probes confirmed colocalization of Cu, Ca and P, and we conclude that this compartment is indeed related to the previously described acidocalcisome, although we wonder whether in any one cell, there may be different types of acidocalcisomes housing different concentrations of individual metals. By analogy to zincosomes described in worms and animal cells and Zn-accumulating lysosome-related organelles, it may be useful to refer to the $Cu^+$-containing compartments as cuprosomes[22,43–46].

Researchers have previously found foci of Cu accumulation, for example, in cells of Wilson disease patients; in the $Ctr^{int/int}$ mouse, where intestinal epithelial cells contain sites of Cu concentration; and in mouse fibroblasts lacking metallothionein and Atox1 (refs. 47,48). In these situations, there also were high concentrations of biologically unavailable Cu. The recapitulation of this phenotype in *C. reinhardtii* provided an excellent opportunity to use a genetic approach to dissect the mechanism of formation of the Cu-loaded compartment and the pathways of Cu mobilization from these compartments. At present, the identities of the transporters that load and unload $Cu^+$ into and from this lysosome-related organelle are unknown. A proteomic analysis of a purified acidocalcisome from a red alga did identify metal transporters in the boundary membrane, and these are certainly candidates that can be tested[49].

Another important question is which chemical species of Cu is being stored. The microbial experimental system used in this work allowed the generation of a homogenous population of cells with very high Cu content, suitable for application of X-ray spectroscopic approaches. Independent samples generated months apart yielded superimposable XANES spectra, indicating that sequestered Cu was reproducibly organized. The EXAFS analysis suggests mononuclear Cu associated with organic ligands (O or N and S) rather than with polynuclear Cu species. We compared the spectra to those of known compounds (including GSH, polyphosphate and phytochelatins), but the Cu species in this work was distinct from previously characterized species. Although transcriptome profiling indicated upregulation of a phytochelatin synthase, this may be a preemptive mechanism against Zn shock[43] rather than a means for chelating the sequestered $Cu^+$.

Aside from the known function of acidocalcisomes to house elements, such as Ca, P, Fe and Zn, we showed here that this compartment can also house $Cu^+$. More notably, the compartment served as a reservoir of $Cu^+$ that could become bioavailable when the cell required $Cu^+$. The vacuole in yeast is perhaps the most analogous compartment: it stores $Zn^{2+}$ in a situation of excess, but in deficiency it can mobilize the $Zn^{2+}$ and support several rounds of replication in the absence of external Zn[43]. We showed that the same is true for sequestered $Cu^+$. Indeed, even in the presence of extracellular Cu, compartmentalized $Cu^+$ was used with priority over assimilated $Cu^+$ for the biosynthesis of holoplastocyanin. Furthermore, accumulated $Cu^+$ offered a selective advantage to cells when they were faced with nutritional deficiency, consistent with bioavailability of compartmentalized $Cu^+$. We conclude that the metal content of the Cu-accumulating compartment is dynamic and can be used for productive metallation of apoproteins.

Sequestered $Cu^+$ was released when we removed the condition prompting sequestration, namely, $Zn^{2+}$ limitation (**Fig. 5a** and **Supplementary Fig. 11**). The released $Cu^+$ not only was available for holoplastocyanin formation (**Fig. 5d**) but also became visible to CRR1. Transcriptome analysis indicated rapid deactivation of the Cu regulon coincident with accumulation of holoplastocyanin (**Fig. 6**). This accounted for decreased $Cu^+$ uptake capacity as a function of time after Zn addition (**Fig. 5d**). In contrast, $Cu^+$ handling components (PCC1 and ATX1 for delivery of the metal to the chloroplast or secretory pathway) were instead upregulated, consistent with redistribution of intracellular $Cu^+$.

We wondered why cells might want to sequester Cu when they are Zn deficient. One possibility is that this occurred to prevent mismetallation of $Zn^{2+}$ sites in enzymes. In the absence of a specific mechanism for $Zn^{2+}$ delivery to these enzymes, low intracellular concentrations of $Zn^{2+}$ might allow binding of $Cu^+$, which would be more competitive for binding to these sites. This is true for the SBP domain of CRR1, which binds $Cu^+$ with $10^5$-fold higher affinity relative to $Zn^{2+}$ (ref. 16). Indeed, in *Euglena gracilis*, Zn deficiency results in misincorporation of Cu instead of Zn into an endonuclease, rendering it inactive[50]. Sequestration of $Cu^+$ would remove the more competitive metal species and allow trace levels of $Zn^{2+}$ to metallate critical proteins, such as those involved in nucleic acid transactions. Another possibility is that Cu is transiently delivered to this compartment en route to its final destination, but in Zn deficiency egress it is blocked or inhibited. This may occur if the transport from the compartment requires $Zn^{2+}$ or if the cytoplasmic Zn/Cu ratio regulates efflux. Regardless, this work underscores the interplay between multiple metal homeostasis pathways.

Received 25 March 2014; accepted 5 September 2014;
published online 26 October 2014 ; corrected after print 6 January 2015

## METHODS

Methods and any associated references are available in the online version of the paper.

**Accession codes.** Gene Expression Omnibus: We deposited the raw reads and expression estimates from the RNA-seq experiment under accession number GSE58786.

## References


1. Andreini, C., Bertini, I., Cavallaro, G., Holliday, G.L. & Thornton, J.M. Metal ions in biological catalysis: from enzyme databases to general principles. *J. Biol. Inorg. Chem.* **13**, 1205–1218 (2008).
2. Irving, H. & Williams, R.J.P. 637. The stability of transition-metal complexes. *J. Chem. Soc.* 3192–3210 (1953).
3. Dudev, T. & Lim, C. Metal binding affinity and selectivity in metalloproteins: insights from computational studies. *Annu. Rev. Biophys.* **37**, 97–116 (2008).
4. Waldron, K.J., Rutherford, J.C., Ford, D. & Robinson, N.J. Metalloproteins and metal sensing. *Nature* **460**, 823–830 (2009).
5. Rae, T.D., Schmidt, P.J., Pufahl, R.A., Culotta, V.C. & O'Halloran, T.V. Undetectable intracellular free copper: the requirement of a copper chaperone for superoxide dismutase. *Science* **284**, 805–808 (1999).
6. Valentine, J.S. & Gralla, E.B. Delivering copper inside yeast and human cells. *Science* **278**, 817–818 (1997).
7. Tottey, S. *et al.* Protein-folding location can regulate manganese-binding versus copper- or zinc-binding. *Nature* **455**, 1138–1142 (2008).
8. Waldron, K.J. & Robinson, N.J. How do bacterial cells ensure that metalloproteins get the correct metal? *Nat. Rev. Microbiol.* **7**, 25–35 (2009).
9. Boal, A.K. & Rosenzweig, A.C. Structural biology of copper trafficking. *Chem. Rev.* **109**, 4760–4779 (2009).
10. Foster, A.W. & Robinson, N.J. Promiscuity and preferences of metallothioneins: the cell rules. *BMC Biol.* **9**, 25 (2011).
11. Merchant, S.S. *et al.* Between a rock and a hard place: trace element nutrition in *Chlamydomonas*. *Biochim. Biophys. Acta* **1763**, 578–594 (2006).
12. Page, M.D., Kropat, J., Hamel, P.P. & Merchant, S.S. Two *Chlamydomonas* CTR copper transporters with a novel Cys-Met motif are localized to the plasma membrane and function in copper assimilation. *Plant Cell* **21**, 928–943 (2009).
13. Merchant, S. & Bogorad, L. Metal ion regulated gene expression: use of a plastocyanin-less mutant of *Chlamydomonas reinhardtii* to study the Cu(II)-dependent expression of cytochrome *c*-552. *EMBO J.* **6**, 2531–2535 (1987).
14. Merchant, S., Hill, K. & Howe, G. Dynamic interplay between two copper-titrating components in the transcriptional regulation of cyt *c*6. *EMBO J.* **10**, 1383–1389 (1991).
15. Kropat, J. *et al.* A regulator of nutritional copper signaling in *Chlamydomonas* is an SBP domain protein that recognizes the GTAC core of copper response element. *Proc. Natl. Acad. Sci. USA* **102**, 18730–18735 (2005).
16. Sommer, F. *et al.* The CRR1 nutritional copper sensor in *Chlamydomonas* contains two distinct metal-responsive domains. *Plant Cell* **22**, 4098–4113 (2010).
17. Malasarn, D. *et al.* Zinc deficiency impacts $CO_2$ assimilation and disrupts copper homeostasis in *Chlamydomonas reinhardtii*. *J. Biol. Chem.* **288**, 10672–10683 (2013).
18. Ghosal, S. *et al.* Imaging and 3D elemental characterization of intact bacterial spores by high-resolution secondary ion mass spectrometry. *Anal. Chem.* **80**, 5986–5992 (2008).
19. Slaveykova, V.I., Guignard, C., Eybe, T., Migeon, H.-N. & Hoffmann, L. Dynamic NanoSIMS ion imaging of unicellular freshwater algae exposed to copper. *Anal. Bioanal. Chem.* **393**, 583–589 (2009).
20. Docampo, R., de Souza, W., Miranda, K., Rohloff, P. & Moreno, S.N.J. Acidocalcisomes—conserved from bacteria to man. *Nat. Rev. Microbiol.* **3**, 251–261 (2005).
21. Eide, D.J. Zinc transporters and the cellular trafficking of zinc. *Biochim. Biophys. Acta* **1763**, 711–722 (2006).
22. Roh, H.C., Collier, S., Guthrie, J., Robertson, J.D. & Kornfeld, K. Lysosome-related organelles in intestinal cells are a zinc storage site in *C. elegans*. *Cell Metab.* **15**, 88–99 (2012).
23. Gudipaty, S.A., Larsen, A.S., Rensing, C. & McEvoy, M.M. Regulation of Cu(I)/Ag(I) efflux genes in *Escherichia coli* by the sensor kinase CusS. *FEMS Microbiol. Lett.* **330**, 30–37 (2012).
24. Fu, Y. *et al.* A new structural paradigm in copper resistance in *Streptococcus pneumoniae*. *Nat. Chem. Biol.* **9**, 177–183 (2013).
25. Rosen, B.P. Transport and detoxification systems for transition metals, heavy metals and metalloids in eukaryotic and prokaryotic microbes. *Comp. Biochem. Physiol. A Mol. Integr. Physiol.* **133**, 689–693 (2002).
26. Castruita, M. *et al.* Systems biology approach in *Chlamydomonas* reveals connections between copper nutrition and multiple metabolic steps. *Plant Cell* **23**, 1273–1292 (2011).
27. Dodani, S.C. *et al.* Calcium-dependent copper redistributions in neuronal cells revealed by a fluorescent copper sensor and X-ray fluorescence microscopy. *Proc. Natl. Acad. Sci. USA* **108**, 5980–5985 (2011).
28. Banci, L., Bertini, I., Cantini, F. & Ciofi-Baffoni, S. Cellular copper distribution: a mechanistic systems biology approach. *Cell. Mol. Life Sci.* **67**, 2563–2589 (2010).
29. Corazza, A., Harvey, I. & Sadler, P.J. 1H, 13C-NMR and X-ray absorption studies of copper(I) glutathione complexes. *Eur. J. Biochem.* **236**, 697–705 (1996).
30. Kropat, J. *et al.* A revised mineral nutrient supplement increases biomass and growth rate in *Chlamydomonas reinhardtii*. *Plant J.* **66**, 770–780 (2011).
31. Lieberman, R.L. *et al.* Characterization of the particulate methane monooxygenase metal centers in multiple redox states by X-ray absorption spectroscopy. *Inorg. Chem.* **45**, 8372–8381 (2006).
32. Chauhan, S., Kline, C.D., Mayfield, M. & Blackburn, N.J. Binding of copper and silver to single-site variants of peptidylglycine monooxygenase reveals the structure and chemistry of the individual metal centers. *Biochemistry* **53**, 1069–1080 (2014).
33. Aschar-Sobbi, R. *et al.* High sensitivity, quantitative measurements of polyphosphate using a new DAPI-based approach. *J. Fluoresc.* **18**, 859–866 (2008).
34. Ruiz, F.A., Marchesini, N., Seufferheld, M., Govindjee & Docampo, R. The polyphosphate bodies of *Chlamydomonas reinhardtii* possess a proton-pumping pyrophosphatase and are similar to acidocalcisomes. *J. Biol. Chem.* **276**, 46196–46203 (2001).
35. Rea, P.A. & Poole, R.J. Vacuolar $H^+$-translocating pyrophosphatase. *Annu. Rev. Plant Physiol. Plant Mol. Biol.* **44**, 157–180 (1993).
36. Bickmeyer, U., Grube, A., Klings, K.-W. & Köck, M. Ageladine A, a pyrrole-imidazole alkaloid from marine sponges, is a pH sensitive membrane permeable dye. *Biochem. Biophys. Res. Commun.* **373**, 419–422 (2008).
37. Huang, G. *et al.* Adaptor protein-3 (AP-3) complex mediates the biogenesis of acidocalcisomes and is essential for growth and virulence of *Trypanosoma brucei*. *J. Biol. Chem.* **286**, 36619–36630 (2011).
38. Blaby-Haas, C.E. & Merchant, S.S. The ins and outs of algal metal transport. *Biochim. Biophys. Acta* **1823**, 1531–1552 (2012).
39. La Fontaine, S. *et al.* Copper-dependent iron assimilation pathway in the model photosynthetic eukaryote *Chlamydomonas reinhardtii*. *Eukaryot. Cell* **1**, 736–757 (2002).
40. Chen, J.C., Hsieh, S.I., Kropat, J. & Merchant, S.S. A ferroxidase encoded by *FOX1* contributes to iron assimilation under conditions of poor iron nutrition in *Chlamydomonas*. *Eukaryot. Cell* **7**, 541–545 (2008).
41. Horng, Y.-C., Cobine, P.A., Maxfield, A.B., Carr, H.S. & Winge, D.R. Specific copper transfer from the Cox17 metallochaperone to both Sco1 and Cox11 in the assembly of yeast cytochrome *c* oxidase. *J. Biol. Chem.* **279**, 35334–35340 (2004).
42. Remacle, C. *et al.* Knock-down of the *COX3* and *COX17* gene expression of cytochrome *c* oxidase in the unicellular green alga *Chlamydomonas reinhardtii*. *Plant Mol. Biol.* **74**, 223–233 (2010).
43. Simm, C. *et al.* *Saccharomyces cerevisiae* vacuole in zinc storage and intracellular zinc distribution. *Eukaryot. Cell* **6**, 1166–1177 (2007).
44. Palmiter, R.D. & Huang, L. Efflux and compartmentalization of zinc by members of the SLC30 family of solute carriers. *Pflugers Arch.* **447**, 744–751 (2004).
45. MacDiarmid, C.W., Gaither, L. & Eide, D. Zinc transporters that regulate vacuolar zinc storage in *Saccharomyces cerevisiae*. *EMBO J.* **19**, 2845–2855 (2000).
46. Miyabe, S., Izawa, S. & Inoue, Y. The Zrc1 is involved in zinc transport system between vacuole and cytosol in *Saccharomyces cerevisiae*. *Biochem. Biophys. Res. Commun.* **282**, 79–83 (2001).
47. Miyayama, T., Suzuki, K.T. & Ogra, Y. Copper accumulation and compartmentalization in mouse fibroblast lacking metallothionein and copper chaperone, Atox1. *Toxicol. Appl. Pharmacol.* **237**, 205–213 (2009).
48. Ralle, M. *et al.* Wilson disease at a single cell level: intracellular copper trafficking activates compartment-specific responses in hepatocytes. *J. Biol. Chem.* **285**, 30875–30883 (2010).
49. Yagisawa, F. *et al.* Identification of novel proteins in isolated polyphosphate vacuoles in the primitive red alga *Cyanidioschyzon merolae*. *Plant J.* **60**, 882–893 (2009).
50. Czupryn, M., Falchuk, K.H., Stankiewicz, A. & Vallee, B.L. A *Euglena gracilis* endonuclease zinc endonuclease. *Biochemistry* **32**, 1204–1211 (1993).


## Acknowledgments

This work is supported, in part, by grants from the US National Institutes of Health (NIH; GM42143 and GM092473 to S.S.M., DK068139 to T.L.S. and GM079465 to C.J.C.), the United States Department of Energy Cooperative Agreement (DE-FC02-02ER63421 to D. Eisenberg for support of J.A.L.) and the German Academic Exchange Service DAAD (D0847579 to A.H.-H. and D1242134 to M.M.). Work at Lawrence Livermore National Laboratory (LLNL) was performed under the auspices of the US Department of Energy at LLNL under contract DE-AC52-07NA27344, with funding provided by the US Department of Energy Genomic Science Program under contract SCW1039. Portions of this research were carried out at the Stanford Synchrotron Radiation Lightsource (SSRL). SSRL is a national user facility operated by Stanford University, and the SSRL Structural Molecular Biology Program is supported by the Department of Energy–Office of Biological and Environmental Research and by the NIH–National Center for Research Resources Biomedical Technology Program. D.B. is supported by the NIH (T32HL120822), and C.J.C. is an investigator with the Howard Hughes Medical Institute. Electron microscopy was performed at the Electron Microscopy Services Center of the University of California–Los Angeles Brain Research Institute. We thank A. Aron and K.M. Ramos-Torres for their help with resynthesis and optical spectroscopy of fresh CS3 and Ctrl-CS3 for control experiments.

## Author contributions

S.S.M., A.H.-H. and M.M. designed experiments. A.H.-H., M.M. and J.K. cultured cells and supplied samples for NanoSIMS, X-ray absorption spectroscopy (XAS) and RNA-seq. M.M. and J.K. measured cellular metal contents by ICP-MS. A.H.-H. performed immunoblotting and qRT-PCR for expression analysis. A.H.-H. and M.M. imaged cells by confocal and electron microscopy and analyzed the resulting data. J.P.-R., P.K.W. and M.M. analyzed intracellular metal distribution by NanoSIMS, and D.B. and T.L.S. collected and analyzed XAS data. M.M. isolated Cu-containing compartments and did the Cu isotope labeling experiments in conjunction with LC-ICP-MS analysis. D.I.S. and M.M. performed quantitative MS of protein fractions under the supervision of J.A.L. S.D.G. prepared RNA-seq libraries and analyzed the resulting data. S.C.D., D.W.D. and J.C. synthesized the $Cu^+$-sensitive CS3 dye (and control) under the supervision of C.J.C., M.M. and S.S.M., and A.H.-H. wrote the manuscript with input from J.C. and P.K.W.

## Competing financial interests

The authors declare no competing financial interests.

## Additional information

Supplementary information and chemical compound information is available in the online version of the paper. Reprints and permissions information is available online at http://www.nature.com/reprints/index.html. Correspondence and requests for materials should be addressed to S.S.M.

## ONLINE METHODS

**Strains and cultures.** The *C. reinhardtii* strains CC-4532 (wild-type) and CC-3960 *(crr1-2)* are available at the *C. reinhardtii* culture collection (http://www.chlamy.org/). We also used two independent transformants of *crr1-2* with pARG7.8 (*crr1*a and *crr1*b), and two independent transformants of the complementation strain containing both pARG7.8 and pCRR1 (CRR1a and CRR1b) were used as a control[16].

Unless noted otherwise, algae were grown from an inoculum of $1 \times 10^5$ cells/ml in Tris-acetate-phosphate (TAP) medium containing our revised micronutrient composition[30] at 24 °C under continuous light (~90 µmol $m^{-2}$ $s^{-1}$) with shaking (180 r.p.m.)[51]. To establish the light spectrum, as shown in **Supplementary Figure 19**, we used two cool white fluorescent bulbs at 4,100 K for each one warm white fluorescent bulb at 3,000 K.

For studying metal-defined conditions, all glassware was triple washed in 6 N hydrochloric acid followed by at least six rinses in Milli-Q purified (Millipore) water. Zn limitation was induced by inoculating cells from a nutrient-replete culture to $10^5$ cells/ml into 100-ml culture medium without supplemented Zn ('first round culture') and then into medium without supplemented Zn ('second round culture'). $ZnCl_2$ was resupplied at 2.5 µM to these limited cultures where described when they reached a density of $1 \times 10^6$ cells/ml ('$t_{0h}$' of Zn resupply). For control samples, Cu deficiency was induced similarly by omitting Cu during media preparation.

**Growth rate determination.** Triplicate first- and second-round cultures of the wild-type strain were grown as described above, and samples were counted every 24 h by light microscopy using a hemocytometer (Hausser Scientific).

**Quantitative metal and phosphorus content analysis of cells and Cu-accumulating compartments.** A total number of $1 \times 10^8$ cells was collected by centrifugation at 1,700*g* for 10 min and washed once in 1 mM $Na_2$-EDTA to remove cell surface–associated metals and once in Milli-Q water. The washed cell paste was overlaid with nitric acid of 24% (v/v) in 1 ml and digested at 65 °C for about 12 h. The cell hydrolysate was diluted in corresponding to a final concentration Milli-Q water to a final nitric acid concentration of 2.4% (v/v). These measurements were repeated routinely to determine the cellular Cu content of all cells that were used for other experiments, such as NanoSIMS analysis, XAS and confocal microscopy.

Isolated compartments were collected at 5,000*g* for 20 min to a total number of $10^9$ per analyzed condition and were treated as described above. Aliquots of fresh or spent culture medium were treated with nitric acid to a final concentration of 2.4% (v/v). To obtain corresponding blank samples, the volume of cell hydrolysate, Cu enriched hydrolysate or culture medium was replaced by Milli-Q water and treated as described above. Total metal and phosphorous contents were measured by inductively coupled plasma MS (ICP-MS) on an Agilent 7500ce instrument, and quantification was done by using appropriate calibration standards (ICP Supplies).

**NanoSIMS analysis.** We used the LLNL Cameca NanoSIMS 50 (Gennevilliers, France) to image the intracellular distribution of bound Ca, Cu and Zn[18,19,52]. Cells from three independent cultures that were grown for 3 d in Zn-limited medium or cultured during Zn resupply were collected by centrifugation and immersed in a solution containing 2% glutaraldehyde and 2% paraformaldehyde in 0.1 M PBS, pH 7.4, for 2 h at room temperature and then incubated at 4 °C. Subsequently, 0.5% of tannic acid was added to the cells and incubated for 1 h at room temperature. The cells were washed five times in 0.1 M PBS buffer and post-fixed in a solution of 1% $OsO_4$ in PBS, pH 7.2–7.4. The samples were washed four times in Na-acetate buffer, pH 5.5. The samples were dehydrated in an ethanol gradient (50 %, 75 %, 95 %, 100 %, 100 % and 100%) for 10 min each, passed through propylene oxide and infiltrated for 2 h first in a 1:1 mixture of Epon 812 and propylene oxide and then in a 2:1 mixture for 2 h. The cells were then infiltrated in pure Epon 812 overnight and cured in an oven at 60 °C for 48 h. Sections of 200-nm thickness (gray interference color) were cut on an ultramicrotome (RMC MTX) using a diamond knife and deposited on 200 mesh carbon-coated molybdenum grids. Sectioned cells were first located and imaged by STEM or TEM. Then they were relocated and analyzed in the NanoSIMS 50. A focused negative oxygen ion primary beam was scanned over the sample (256 × 256 pixels, 25–100 µm² raster) to generate secondary ions. The secondary ion mass spectrometer was tuned to ~5,000 mass resolving power, and $^{12}C^+$, $^{40}Ca^+$, $^{63}Cu^+$ and $^{66}Zn^+$ were detected simultaneously by electron multipliers in pulse counting mode. The correct metal ion peaks were identified using NBS610 glass (National Institute of Standards and Technology, USA). Each analysis area was scanned 10 to 20 times to collect serial secondary ion images for quantification.

The NanoSIMS ion image data were processed using custom software (LIMAGE, L.R. Nittler, Carnegie Institute of Washington, USA). The ion images were corrected for detector dead time and image shifts between scans and then used to produce ion ratio images. For defined regions of interest (either whole cell areas or areas of Cu accumulation), ion ratios were calculated for $^{40}Ca^+/^{12}C^+$, $^{63}Cu^+/^{12}C^+$ and $^{66}Zn^+/^{12}C^+$ by averaging the replicate scans[18,19,52]. These data provide relative quantitative composition, but they were not standardized to provide concentration data.

**Cu isotope labeling.** For labeling with >98.5% enriched $^{63}Cu$ or $^{65}Cu$ isotopes (Cambridge Isotope Laboratories, Inc.), all media were prepared by using either $^{63}CuCl_2$ or $^{65}CuCl_2$ (at 2 µM initial concentration) as the sole Cu source. Cells were grown for at least 12 generations in the presence of the enriched Cu source. Upon resupply of Zn in the second-round cultures, the other enriched Cu isotope was added at fivefold molar excess (10 µM) to these cultures either directly or 5 h after the addition of Zn. Cells were collected at 0 h, 10 h, 24 h and 60 h for LC-ICP-MS analysis of soluble proteins (see growth curves and sampling scheme in **Supplementary Fig. 15a**) by centrifugation (4,000*g* at 4 °C for 10 min) and washed twice with Millipore water. Further samples from the same cultures were taken for quantitative ICP-MS to analyze the Cu isotope content of both cell pellets (aliquots of $10^8$ cells) and medium supernatant. The cell pellets were washed twice with 2.5 mM $Na_2$-EDTA and once with Millipore water to remove remaining metal salts from the cell surface.

**Work under anaerobic conditions.** All anaerobic work was carried out in an airtight glove box (Coy Laboratories) containing a controlled $H_2$ (3%)/$N_2$ (97%) atmosphere. Solutions and plastic ware were allowed to equilibrate for at least 6 h inside the anaerobic chamber before usage. Buffer solutions for HPLC were made anoxic by purging them with forming gas overnight.

**Protein preparation for metalloprotein analysis.** Collected cells were resuspended under anaerobic conditions in anoxic chromatographic analysis buffer (20 mM Tris, pH 7.5, 20 mM KCl) to equal densities of $10^8$ cells/ml. Work under anaerobic atmosphere was continued during the whole experimental process to preserve the native metal oxidation states. For the quantitative release of soluble proteins including plastocyanin[53,54], two slow freeze (–80 °C) and thaw (20 °C) cycles for cell lysis were carried out in closed and sealed tubes. Supernatant and cell pellets were separated by centrifugation at 20,000*g* at 4 °C for 15 min. To remove insoluble membrane fractions remaining in the supernatant, ultracentrifugation (250,000*g* at 4 °C for 1 h) was done in tubes closed by heat melting. The clear supernatant (with a total protein content of ~1 mg/ml) was then subjected to subsequent protein fractionation and metal content analysis by HPLC-ICP-MS (see below).

**Metalloprotein analysis by HPLC-ICP-MS.** Isotope-specific metalloprotein analysis was performed by high-performance LC (HPLC) linked with inductively-coupled plasma MS (ICP-MS). Aliquots of total soluble protein (~0.5 mg) prepared from different cell samples were injected manually into a bioinert Agilent 1260 HPLC system (Agilent Technologies) that was equilibrated inside an anaerobic chamber (Coy Laboratories). The protein crude extracts were separated anaerobically in 20 mM Tris-Cl, pH 7.5, 20 mM KCl at 25 °C and at a flow rate of 0.5 ml/min via size exclusion chromatography on a 7.5 mm × 30 cm TSKgel G3000SW column (Tosoh). The eluent stream was subjected to a split flow, directing it to the source of the ICP-MS for online metal analysis using the high matrix interface as well as to the HPLC fraction collector for subsequent protein species analysis by immunoblotting and MS. ICP-MS analysis was run in the helium gas mode with time-resolved analysis to minimize signal suppression in the presence of higher salt content. Isotope-specific ion chromatograms were obtained for $^{65}Cu$ and $^{63}Cu$ upon extraction from the total ion signals. The protein elution profiles were recorded by a multi-wavelength detector at 280 nm using a 500-nm reference signal. The delay time between UV-vis detection of the protein species and the detection of associated metal cofactor(s) by ICP-MS was ~1.6 min, which was also confirmed by using Cu-Zn superoxide dismutase (Sigma Aldrich) as well as purified *C. reinhardtii* plastocyanin as a metalloprotein standard (**Supplementary Fig. 13**).

**Electron microscopy.** Cells and Cu-accumulating compartments were prepared for electron microscopy as described for NanoSIMS analysis above. Sections of 60-nm thickness (gray interference color) were cut on an ultramicrotome (RMC MTX) using a diamond knife. The sections were deposited on single-hole grids coated with Formvar and carbon and double-stained in aqueous solutions of 8% uranyl acetate for 25 min at 60 °C and lead citrate for 3 min at room temperature. Thin sections were examined with a 100CX JEOL (80 kV) electron microscope. For NanoSIMS studies, samples were prepared without uranyl acetate and lead citrate stainings, and 200-nm sections were cut and deposited on molybdenum grids, which were carbon-coated before analysis. ImageJ software was used to manually define and measure whole-cell areas and electron-dense structures. The ratio of electron-dense structure to whole-cell area is given as percentage. Cells from three independent Zn-replete or Zn-limited cultures were analyzed. 55 Zn-limited cells and 79 Zn-replete cells were analyzed. Kruskal-Wallis one-way analysis of variance on ranks was used to determine the statistical significance of the data ($P < 0.001$). For TEM analysis of the Zn resupply time course, we analyzed 45 cells at $t = 0$ h, 32 cells at $t = 10$ h, 40 cells at $t = 24$ h, 42 cells at $t = 60$ h, 35 cells from the Zn-replete culture (early) and 28 cells from the Zn-replete culture (late).

**RNA-Seq.** RNA was extracted from Zn-limited cells and at 1.5 h, 3 h, 4.5 h, 12 h and 24 h after Zn resupply, as described above. Two Zn-replete samples were collected as controls: one from the mid-logarithmic phase and the other from the stationary phase.

Quadruplicate cDNA libraries from each time point were prepared using the TruSeq Stranded mRNA Sample Prep Kit (Illumina) following the manufacturer's instructions (Revision D). Sequencing was performed on a HiSeq 2000 high-throughput sequencer (Illumina) according to the manufacturer's instructions. Eight libraries were loaded per lane and sequenced for 50 nt. After demultiplexing, yields were $2.5 \times 10^7$ reads on average per library. Quality scores were high, averaging between 33 and 40 over the length of the reads. The resulting reads were aligned to v5.3.1 of the *C. reinhardtii* genome assembly[1], available from the Joint Genome Institute at http://www.phytozome.net/. Alignments were performed using TopHat2 (ref. 55) with guidance from the Augustus 11.6 gene models (http://www.phytozome.net/). Expression was quantified and standardized in terms of fragments per kb of exon per million fragments (FPKMs) by Cufflinks, and differential expression testing was performed by Cuffdiff[56].


51. Harris, E.H., Stern, D.B. & Witman, G.B. *The Chlamydomonas Sourcebook: Introduction to Chlamydomonas and its Laboratory Use* (Academic Press, 2009).
52. Chandra, S. in *The Encyclopedia of Mass Spectrometry* (eds. Gross, M. & Caprioli, R.) 469–480 (Elsevier, 2010).
53. Merchant, S. & Bogorad, L. Regulation by copper of the expression of plastocyanin and cytochrome *c*552 in *Chlamydomonas reinhardi*. *Mol. Cell. Biol.* **6**, 462–469 (1986).
54. Li, H.H. & Merchant, S. Degradation of plastocyanin in copper-deficient *Chlamydomonas reinhardtii*. Evidence for a protease-susceptible conformation of the apoprotein and regulated proteolysis. *J. Biol. Chem.* **270**, 23504–23510 (1995).
55. Kim, D. *et al.* TopHat2: accurate alignment of transcriptomes in the presence of insertions, deletions and gene fusions. *Genome Biol.* **14**, R36 (2013).
56. Trapnell, C. *et al.* Transcript assembly and quantification by RNA-Seq reveals unannotated transcripts and isoform switching during cell differentiation. *Nat. Biotechnol.* **28**, 511–515 (2010).






doi:10.1038/nchembio.1662

ERRATUM

# Subcellular metal imaging identifies dynamic sites of Cu accumulation in *Chlamydomonas*

Anne Hong-Hermesdorf, Marcus Miethke, Sean D Gallaher, Janette Kropat, Sheel C Dodani, Jefferson Chan, Dulmini Barupala, Dylan W Domaille, Dyna I Shirasaki, Joseph A Loo, Peter K Weber, Jennifer Pett-Ridge, Timothy L Stemmler, Christopher J Chang & Sabeeha S Merchant

*Nat. Chem. Biol.* **10**, 1034–1042 (2014); published online 26 October 2014; corrected after print 6 January 2015

In the version of this article initially published, the labels in Figure 4b were incorrect. The error has been corrected in the HTML and PDF versions of the article.